Quasi-two-dimensional magnetic properties in atomic layer resolved $La_{0.7}Sr_{0.3}MnO_3/LaAlO_3$ superlattices

Bangmin Zhang,[1,*,†] Hong Zhang,[2,3,*] Xiao Chi,[4] Ping Yang,[4] Jun Ding,[5] Jingsheng Chen,[5] and Gan Moog Chow[5,‡]

[1]*Guangdong Provincial Key Laboratory of Magnetoelectric Physics and Devices, Centre for Physical Mechanics and Biophysics, School of Physics, Sun Yat-Sen University, Guangzhou 510275, China*

[2]*School of Materials and Energy, Electron Microscopy Centre, Lanzhou University, Lanzhou 730000, People's Republic of China*

[3]*School of Materials and Energy, Electron Microscopy Centre, Yunnan University Kunming 650500, People's Republic of China*

[4]*Singapore Synchrotron Light Source (SSLS), National University of Singapore, 5 Research Link, 117603, Singapore*

[5]*Department of Materials Science & Engineering, National University of Singapore, 9 Engineering Drive 1, 117576, Singapore*

(Received 11 June 2021; revised 20 December 2021; accepted 13 February 2023; published 27 February 2023)

Materials in low dimensions show interesting physics and excellent potential in practical applications. The atomic-level control of two-dimensional (2D) behavior in a traditional three-dimensional (3D) system is quite hard, and the $(La_{0.7}Sr_{0.3}MnO_3)_n/(LaAlO_3)_n$ (LMSO/LAO) superlattice on a (001) $SrTiO_3$ substrate was investigated to explore its quasi-2D behavior. The number of magnetic phase transitions has a close relationship with the number of unit cells (n): only one phase transition for $n = 2$ and four phase transitions for $n = 8$. It was found that the local structure of each $La_{0.7}Sr_{0.3}MnO_3$ atomic layer is responsible for the multiple phase transitions: the gradual change of the tetragonal ratio and the in-plane tensile strain-induced $3d$ electronic orbital occupancy control the magnetic properties of 2D-LSMO atomic layers. For the outmost 2D-LSMO atomic layer contacting $LaAlO_3$ directly, interface-related factors reduce the intensity of magnetic interaction significantly. With the increase of n, the properties around the LSMO/LAO interface changes, which demonstrates that the superlattice configuration and the lattice-mismatch strain could be employed to explore the quasi-2D behavior of a traditional 3D system.

DOI: 10.1103/PhysRevB.107.085143

I. INTRODUCTION

Materials in low dimensions have attracted much attention due to their fascinating properties [1,2] and rich physics, such as superconductivity [3] in thin films, phases induced [4] around the interface, and enhanced magnetic properties. Materials in two-dimensional (2D) form, such as ultrathin films and superlattices, have been widely investigated and exploited in different scenarios [5,6] with excellent potential in practical applications. One surprising discovery recently is the superconductivity observed in an infinite-layer nickelate $Nd_{0.8}Sr_{0.2}NiO_2$ film [3], which was obtained by reducing traditional three-dimensional (3D) perovskite nickelate $Nd_{0.8}Sr_{0.2}NiO_3$ film with largely enhanced NiO_2 in-plane antiferromagnetic (AFM) coupling, and the electronic structure with a singly occupied in-plane $3d_{x^2-y^2}$ band was proposed to be essential. Perpendicular to the NiO_2 plane, due to the lack of oxygen, the coupling among cations along this direction is believed to be weak by analogizing to a cuprate superconductor. In addition, around the $SrTiO_3/LaAlO_3$ interface, charge transfer from $LaAlO_3$ to $SrTiO_3$ occurs [7,8], which was constrained in several unit-cell thickness with high in-plane mobility (2D electron gas), which is in sharp contrast to the insulating parent components. Hence, exploring strategies to obtain quasi-2D behavior with limited interlayer magnetic coupling mediated by electrons in a traditional 3D perovskite oxide would be useful to tailor materials properties.

Authors of recent work [9] utilized the superlattice configuration to modulate the ferromagnetic (FM) and AFM coupling between magnetic layers by changing the periodic thickness, which reveals that changing the perpendicular magnetic coupling could induce different phenomena. Manganite in an ABO_3 perovskite structure is a strongly correlated electron system [10] with coupling between crystal structure, spin, charge, and the orbital structure. The electron could move not only in the MnO_2 plane but also transport perpendicular to the MnO_2 plane, where the cations couple with neighboring cations both in the MnO_2 plane and out of plane. Hence, controlling the properties of a $3d$ perovskite at the atomic layer level is not easy due to the strong coupling of cations among different atomic layers. Considering a heterostructural interface with lattice mismatch, the structural coupling with structural connectivity [11] would cause the gradual change of the crystal structure/local structure [12] at the atomic level from the interface to the center of each layer, which might induce variation of the electronic structure and materials properties. In addition, a strained single layer of manganite thin film could induce orbital polarization of $3d$ e_g orbitals, either $3d_{x^2-y^2}$ or $3d_{3z^2-r^2}$ preference [13]. Hence, the superlattice configuration with lattice mismatch strain is worthy of study, to polarize the occupancy of electronic

*These authors contributed equally to this paper.
†zhangbm5@mail.sysu.edu.cn
‡msecgm@nus.edu.sg

orbitals and control the in-plane and out-of-plane magnetic coupling.

In this paper, the $(La_{0.7}Sr_{0.3}MnO_3)_n/(LaAlO_3)_n$ (LSMO/LAO) superlattice with n unit cells for each layer in one period was investigated. The number of magnetic phase transitions (Curie temperature) has a close relationship with the number of unit cells (n): only one phase transition for $n = 2$ and four phase transitions for $n = 8$. Further study shows that each $La_{0.7}Sr_{0.3}MnO_3$ 2D atomic layer with a different local structure was responsible for the multiple phase transitions. The gradual change of the tetragonal ratio and the corresponding $3d$ electronic orbital occupancy control 2D-LSMO atomic layers with the intensity of the magnetic interaction in the progression ratio; for the outmost 2D-LSMO atomic layer contacting $LaAlO_3$ directly, the interface-related factors reduce the intensity of the magnetic interaction significantly. With the change of n, the properties around the LSMO/LAO interface change, which demonstrates that the quasi-2D behavior of the manganite film could be induced in a superlattice with an inhomogeneous local structure, which could be applicable in other 3D systems.

II. EXPERIMENTAL DETAILS

The LSMO/LAO superlattice with n unit cells of $La_{0.7}Sr_{0.3}MnO_3$ or $LaAlO_3$ in each period was grown on a (001) $SrTiO_3$ (STO) substrate by pulsed laser deposition equipped with reflection high-energy electron diffraction to monitor the thickness at 100 mTorr oxygen pressure at a substrate temperature of 780° C. There are two series of superlattices: one is with fixed total thickness 120 u.c., and the other one is with six fixed periods. After deposition, the sample was cooled at 15° C/ min in a 200 mTorr oxygen atmosphere. The energy density of the 248 nm KrF excimer laser beam on the target was $1.5\,J/cm^2$ at a pulse frequency of 2 Hz. The magnetic properties were measured by a superconducting quantum interference device. The crystallographic properties of the films at room temperature were studied using a four-circle diffractometer (Huber 4-circle system 90000-0216/0) at the Singapore Synchrotron Light Source (SSLS), with x-ray wavelength equivalent to Cu $K\alpha_1$ radiation. The polarized x-ray absorption spectrum (XAS) with different incident angles at $L_{3,2}$ edges of Mn were measured at the SINS beamline at SSLS, using total electron mode for data collection. The local structure was measured by high-resolution scanning transmission electron microscopy (HR-STEM) equipped with electron energy loss spectroscopy (EELS).

III. RESULTS AND DISCUSSION

Figure 1 shows magnetization-temperature (MT) curves for LSMO/LAO superlattice with fixed total thickness 120 u.c., n unit cells of each layer in one period, which was measured during the warming process at zero magnetic field after 100 Oe field cooling (FC) from room temperature to 10 K, and the magnetism comes from the LSMO layer. For $n = 2$, there is only one peak from the first-derivative (red) curve of the MT curve, which reveals the phase transition–Curie temperature; with the increase of n, more phase transitions–multiple Curie temperatures appear. Figure 1(d) summarizes the phase transition temperatures with different periodic thickness. The

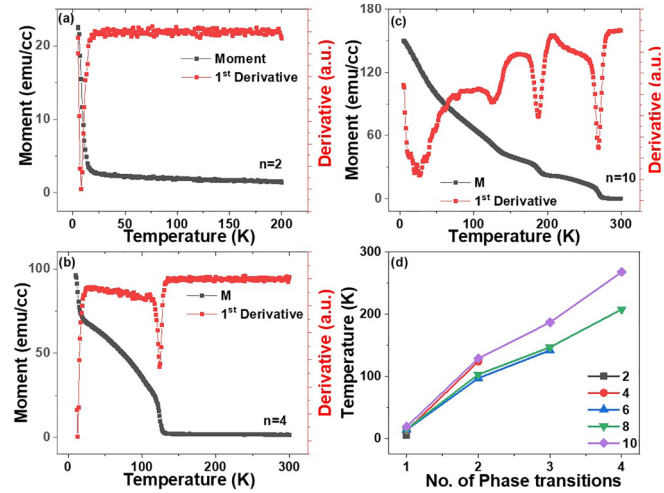

FIG. 1. Magnetization-temperature (MT) curve for (a) $n = 2$, (b) $n = 4$, and (c) $n = 10$ measured during the warming process at zero magnetic field after 100 Oe field cooling from room temperature to 10 K. (d) Summarized phase transition temperatures with different n.

numbers of phase transitions are 1, 2, 3, 4, and 4 for $n = 2$, 4, 6, 8, and 10, respectively. There is a close correlation between the number of phase transitions and the periodic thickness (n): The number of phase transitions is half of the number of LSMO unit cells in each period for $n \leqslant 8$, and the exception with $n = 10$ is discussed later. The total thickness of each superlattice is the same, and the difference in magnetic behavior should correlate with the superlattice configuration, which is characterized by x-ray reflectivity and x-ray diffraction below.

To study whether the number of interfaces (period number) affects the phenomenon, additional superlattices with six fixed periods and $n = 4$ and 6 were fabricated, and the properties are shown in Fig. 2. Including the above sample with $n = 10$ (6 periods), it is found that, in this series with fixed periods, the phenomenon is the same as the above series with fixed total thickness: There are two phase transitions for $n = 4$ and three phase transitions for $n = 6$. This suggests that the number of interfaces (periods) is not the reason for the observed phenomenon. However, the temperature of the phase transition for the $n = 4$ superlattice (6 periods, 48 u.c.) is lower than that of the $n = 4$ superlattice in the series with fixed total thickness (15 periods, 120 u.c.), like what occurs for $n = 6$. Considering the existence of magnetic dipole interactions

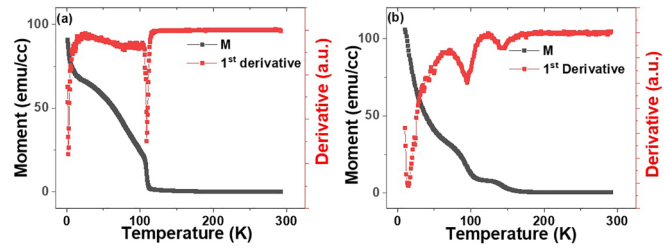

FIG. 2. Magnetization-temperature (MT) curve for (a) $n = 4$ and (b) $n = 6$, with fixed period of 6, measured during warming process at zero magnetic field after 100 Oe field cooling from room temperature to 10 K.

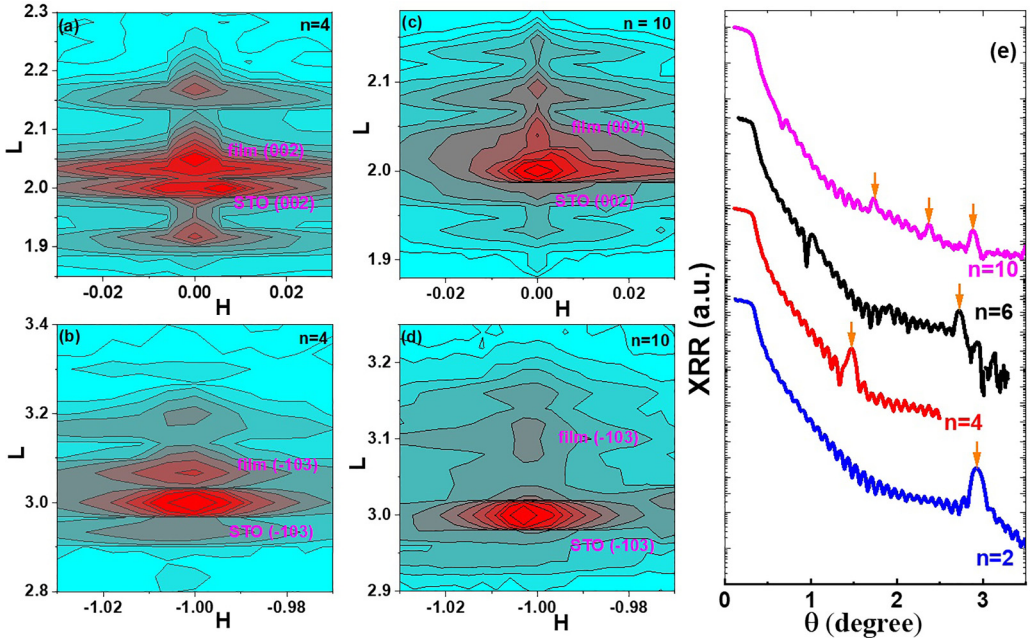

FIG. 3. The (002) and (−103) reciprocal space mapping (RSM) of superlattice with (a) and (b) $n = 4$ and (c) and (d) $n = 10$. (e) X-ray reflectivity for different superlattice.

among different periods in the superlattice [9], the decrease in the transition temperature is attributed to the lower thickness with decreased coupling between periods. The following discussion focuses on the series with fixed total thickness 120 u.c.

Either coexistence of several magnetic phases [14] or the multiple phase transitions [15] in a single magnetic phase may cause the above phenomenon with the decrease in temperature. For a superlattice with different n, the transition temperatures of LSMO are different. If only a single phase of LSMO exists, several factors may cause the appearance of multiple phase transitions with decreasing temperature. (a) The LAO layer: There is no phase transition of LAO <300 K reported, and the LAO layer was fabricated at the same parameters for all superlattices. (b) The LSMO layer: For bulk LSMO, only one PM-to-FM phase transition exists [10], and the LSMO thin film was fabricated at the same parameters for all superlattices. The phase transition temperatures at different n should be the same if the multiple phase transitions came from the single phase of LSMO (and/or the effect of the LAO layer) under the same fabrication parameters. (c) The STO substrate: There is a phase transition at 105 K for STO [16,17], but this temperature is different from the phase transition temperatures observed above. Based on the above discussion, the appearance of multiple phase transitions should have other origins.

If multiple magnetic phases exist, either a 3D magnetic cluster or a 2D-LSMO atomic layer with different magnetic properties may occur. For $n = 2$, the two LSMO atomic layers contacting the LAO directly have the same local environment; for $n = 4$, there are two different local environments: two outmost LSMO atomic layers contacting the LAO directly and two inner LSMO atomic layers. Similarly for $n = 6$ and 8, there are three and four different local environments, respectively. The close correlation between the number of local environments and phase transitions suggests that each 2D-LSMO atomic layer with a different local environment has a corresponding magnetic property, such as phase transition points. For $n = 10$, there are five different local environments, but only four phase transitions occur with decreasing temperature, which suggests that the fourth and fifth local environments of the LSMO atomic layer (central four LSMO atomic layers) have similar magnetic properties or strong interlayer interactions, supported by measured orbital occupancy discussed below. If the 3D magnetic cluster with different magnetic properties is the origin of multiple phase transitions, a difference in the crystal structure could be expected according to the double-exchange model with structural distortion [18]. For example, an observable difference in the crystal structure between $n = 2$ and 8 exists with different Curie temperatures. However, for $n = 8$ with quite large difference among its own four Curie temperatures 15, 110, 143, and 190 K, there is no observable difference in the crystal structure from high-resolution x-ray diffraction (HRXRD) in Figs. 3(a)–3(d). Hence, the 2D-LSMO atomic layers with different local environments are responsible for the multiple phase transitions observed in Fig. 1(d).

To study the large difference in Curie temperature, the crystal structure was investigated by HRXRD. From (002) and (−103) reciprocal space mapping, the in-plane lattice constant is fully clamped by the STO substrate. For different n, the x-ray reflectivity shows peaks [labeled by orange arrows in Fig. 3(e)] due to the reflection of $La_{0.7}Sr_{0.3}MnO_3/LaAlO_3$ interfaces, and multiple small peaks [unlabeled peaks in Fig. 3(e)] due to reflection of film surface and film/substrate interface also appear, indicating the high quality of the interfaces and the formation of a superlattice configuration. The x-ray diffraction also shows satellites peaks, labeled ±1, ±2, … in Figs. 4(a) and 4(b), which is consistent with the x-ray reflectivity results. For $n = 2$, the superlattice shows only one

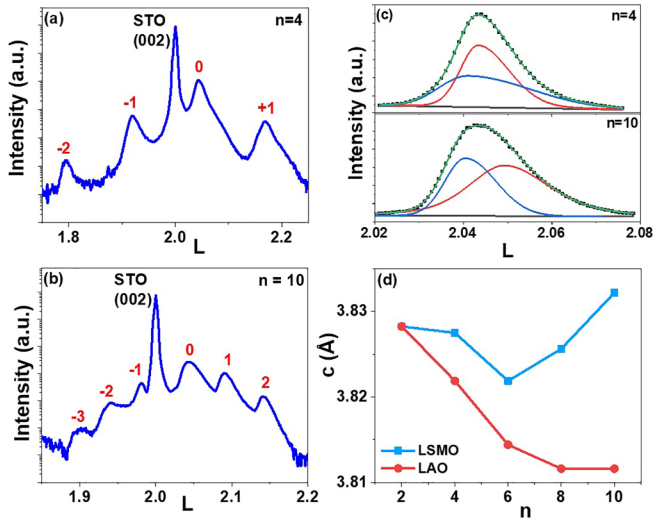

FIG. 4. The (002) L scan for superlattice with (a) $n = 4$ and (b) $n = 10$. (c) The (002) peak and corresponding fitting for $n = 4$ and 10; the red and blue fitted curves correspond two separated structures, and the green curve is the sum of them; the black dots are measured results. (d) Summarized out-of-lattice constant of LSMO and LAO parts in superlattice with different n.

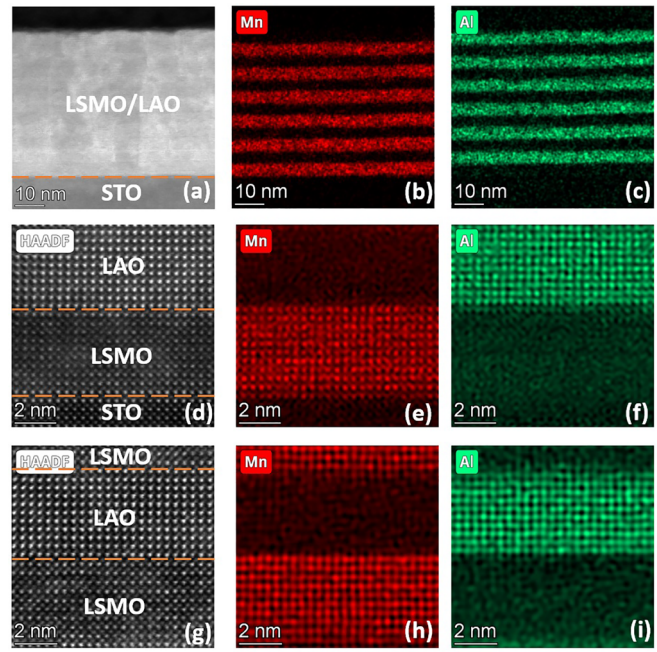

FIG. 5. (a)–(c) Low-resolution transmission electron microscopy (TEM) image and corresponding electron energy loss spectroscopy (EELS) mapping for $n = 10$; and the high-resolution TEM image and corresponding EELS mapping (d)–(f) around the STO/superlattice interface and (g)–(i) at the center of the superlattice.

(002) peak. However, for $n > 2$, the main peak (zeroth order) of the (002) L scan is asymmetric, which could be well fitted by two separated subpeaks even though no strain relaxation occurs, as shown in Fig. 4(c). Previous work [19] has shown that, in a superlattice with large thickness of two components in one period, each component forms one peak in the x-ray diffraction; with the decrease of thickness, these two independent peaks move toward each other, and the asymmetry of the zeroth-order peak appears before finally merging into one symmetric peak. The pseudocubic lattice constants are 3.880 Å for bulk LSMO [20] and 3.790 Å for bulk LAO [13], which are smaller than that of the STO substrate 3.905 Å. Under in-plane tensile strain, the out-of-plane lattice constant c would decrease for both LSMO and LAO layers. Hence, with the in-plane lattice constant fully clamped by the STO substrate, the main contribution to the left subpeak with larger c is attributed to the LSMO layer and the right one to the LAO layer, due to the larger pseudocubic lattice constant of bulk LSMO than that of bulk LAO. The summarized c of the LSMO and LAO layers is shown in Fig. 4(d). For LAO, the averaged c_{LAO} decreases with the increase of n and gets to its equilibrium value for $n > 6$. For LSMO, with the increase of n, the averaged c_{LSMO} decreases first and then increases for $n > 6$. The different behavior between LSMO and LAO should be due to their intrinsic properties, and the following focuses on its effect on materials properties.

HR-STEM and EELS have been employed to study the local structure of the superlattice. Figure 5(a) shows the EELS mapping of the whole cross-section of the superlattice with $n = 10$, and the LAO and LSMO layers separate from each other clearly, consistent with the nominal structure. The atomic-resolved high-resolution EELS mapping around the substrate/superlattice interface and the center of the superlattice in Figs. 5(b) and 5(c) show that the LSMO/LAO interfaces are good quality, although atomic diffusion occurs in ~ 1 atomic layer, commonly observed in film fabricated at high temperature. From the HR-STEM image, the in-plane lattice constant was clamped by the substrate, and the trend of the out-of-plane lattice constant c was summarized in Figs. 6(a) and 6(b). For LSMO around the substrate in the first LSMO layer, c is close to that of the STO substrate due to the interfacial coupling, like that reported before [21], then decreases gradually. For other LSMO layers, c is smaller at two LSMO/LAO interfaces and larger at the center of the LSMO

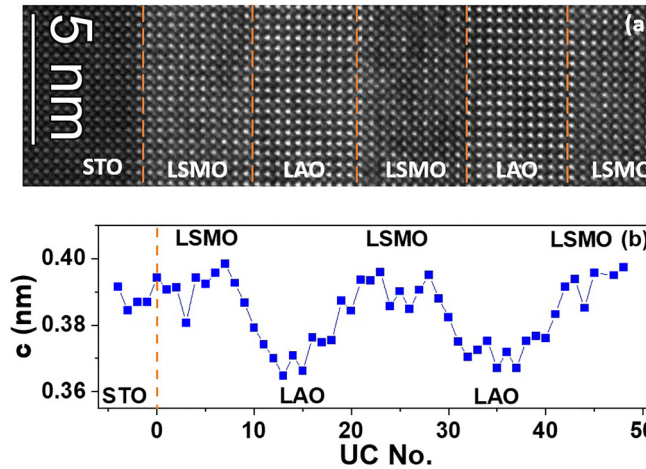

FIG. 6. (a) High-resolution transmission electron microscopy (TEM) image and (b) corresponding trend of the out-of-plane lattice constant.

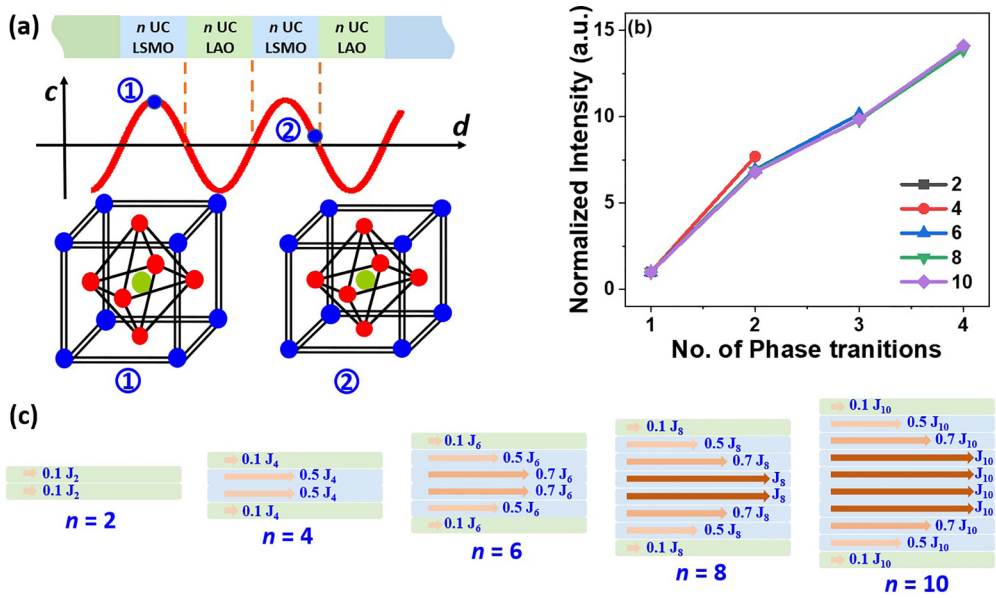

FIG. 7. Illustration of out-of-plane lattice constant in LSMO/LAO superlattice. The lower part shows the change of the tetragonal ratio at different part of LSMO layer; (b) the normalized intensity of magnetic intensity for different magnetic phases; (c) the illustration of intensity of exchange coupling at each LSMO atomic layer for different n. The green bar illustrates the outmost LSMO atomic layer connecting with the LAO atomic layer directly.

layer. For the LAO layer, c is larger at two LAO/LSMO interfaces and smaller at the center of the LAO layer. This trend is important for the materials properties as discussed below.

Across the LSMO/LAO interface, the out-of-plane lattice constant changes gradually from the LAO layer to the LSMO layer. Considering the connectivity around the LSMO/LAO interface [12], the sketch of c for the superlattice is illustrated in Fig. 7(a), which changes gradually around the interface. Due to the clamp of the in-plane lattice constant by the substrate, the tetragonal ratio c/a of the LSMO layer from the interface to the center increases gradually, illustrated in the lower part of Fig. 7(a). According to the double-exchange model with structural distortion [22], the Curie temperature would increase with the tetragonal ratio increasing to 1 due to the electronic delocalization. For fixed n, the local c of LSMO would increase from the LSMO/LAO interface to the center of the LSMO layer. Then the phase transition temperature of the LSMO atomic layer at the LSMO/LAO interface is the lowest, and it should increase gradually to the center of the LSMO layer, which seems consistent with the above discussion on phase transition.

In Fig. 1(c) for $n = 10$, the four transition temperatures are 19, 129, 187, and 268 K. With the averaged strain from x-ray diffraction, the strain-induced change of the phase transition temperature could be described by a phenomenological equation [22,23] $T = T_0(1-\alpha\varepsilon_B-\frac{1}{2}\Delta\varepsilon_{\rm JT}^2)$, where ε_B is the bulk strain, $\varepsilon_{\rm JT}$ is the Jahn-Teller distortion, the Curie temperature of the bulk $T_0 \sim 370$ K, $\alpha\sim10$, and $\Delta \sim 1470$. The calculated Curie temperature for $n = 10$ is ~ 290 K, which is close to the onset of magnetism at the highest phase transition 268 K. With decrease of n, the averaged out-of-plane lattice constant decreases and should induce decreasing temperature of the highest phase transition, which is consistent with experimental results for $n \geqslant 6$. Further decreasing n, the averaged out-of-plane lattice constant increases with decreasing temperature of the highest phase transition, which cannot be explained by strain status and suggests an additional factor should be considered.

Although the phase transition temperatures of the LSMO/LAO superlattice with different periodic thicknesses n are different, an interesting intrinsic relationship among them was observed from quantitative analysis. When the phase transition temperatures for different n were normalized by the lowest phase transition temperature of each superlattice for clarity, it merges into one curve, as shown in Fig. 7(b). Considering that the phase transition temperature reveals the intensity of magnetic exchange coupling J among neighboring Mn ions [14], which tends to align the spins at different Mn ions and stands against the thermal disturbance, this coincidence suggests that, for different superlattices (n), the relative intensity of exchange coupling J in different 2D-LSMO atomic layers has a universal trend. Defining J_n as the intensity of exchange coupling of the central LSMO atomic layer for a superlattice with n unit cells in one period, the intensity profile of exchange coupling in terms of J_n was demonstrated in Fig. 7(c).

Taking $n = 8$ for example, the intensity from the LSMO center to the interface is J_8, $0.7J_8$, $0.5J_8$ ($\sim 0.7 \times 0.7\,J_8$), and $0.1J_8$, respectively, and the coefficient before J_8 comes from the ratio of each transition temperature to the lowest transition point. The intensity of three inner 2D-LSMO atomic layers (local structure) shows geometric progression with the ratio ~ 0.7; for the outmost 2D-LSMO atomic layer connecting with LAO layer directly, the intensity of interaction was significantly reduced. For those < 4 phase transitions ($n = 6,\ 4$), the intensity of exchange coupling of an individual LSMO atomic layer shows the same trend with $0.1J_n$ for the outmost LSMO atomic layer. The missing fourth phase transition with the highest transition temperature does not affect the trend of rest phase transitions, suggesting that the exchange coupling between different 2D-LSMO local environments has limited

effect in these superlattices. Hence, the magnetic properties of a superlattice are dominated by intrinsic properties of each 2D-LSMO atomic layer, of which the universal feature should be sensitive to the local environment.

Combining the above discussion on the crystal structure and the interaction intensity, the magnetic interaction in these superlattices could be understood as below: For $n = 2$, each LSMO atomic layer contacts the LAO layer directly and has quite low intensity of intralayer exchange coupling within the 2D-LSMO atomic layer, which may result from interface-related factors, such as oxygen defects, cation diffusion [24,25], or orbital reconstruction [26] at the heterostructural interface, which is supported by x-ray linear dichroism (XLD) below. With the increase of n, the lowest point of the phase transition is close to that of $n = 2$, and an additional phase transition with a higher transition temperature appears. For $n = 8$, the additional three phase transitions show geometric progression with the ratio ~ 0.7, which suggests the dominant factors for magnetic interactions are similar. Normally, the properties of materials are controlled by the chemical composition and local structure. Then combining the above discussion on the gradual change of the tetragonal ratio and the coincidence between n and the number of phase transitions, the trend of geometric progression should come from the gradual change of the tetragonal ratio: the closer to the center of the LSMO layer, the higher the tetragonal ratio with higher phase transition temperatures [22]. To sum up, the phase transition with the lowest transition temperature is controlled by interface-related factors with significantly reduced intensity of magnetic interaction, and the rest phase transition is mainly controlled by the tetragonal ratio. This could explain the lower onset temperature of magnetism for $n = 2$ with larger averaged c_{LSMO} than that of $n = 6$. Frequently, a superlattice configuration with different periodic thicknesses is employed to increase the interface/bulk ratio and then to control the properties. However, in this paper, we reveal that the change of periodic thickness not only changes the interface/bulk ratio but also the properties of the heterostructural interface, which should be considered to design the superlattice configuration and to explain the results.

The next question is, why does each 2D-LSMO atomic layer behave independently? According to the double-exchange model in manganite, the intensity of exchange coupling depends on the probability of the electron hopping along all directions [27], which relates to the occupancy of the $3d$ e_g orbitals and the local structure. The electronic structure of the superlattice measured by the polarized Mn L edge of XAS to provide more information is shown in Fig. 8(a). For the grazing incident (GI) measurement (incident angle $\theta = 70^\circ$) with the electric field 20° to the normal direction of the film plane, the out-of-plane Mn $3d_{r^2-z^2}$ dominates the absorption, while for the normal incident (NI) measurement (incident angle $\theta = 0^\circ$) with the electric field parallel to the film plane, the in-plane Mn $3d_{x^2-y^2}$ dominates the absorption. The obvious kink ~ 641 eV in both NI and GI measurements for $n = 2$ comes from the Mn^{3+} ion [28,29], and with the increase of n ($\geqslant 4$), the Mn^{3+} signal decreases gradually. With the increase of the chemical valence, both L_3 and L_2 edges shift to a higher-energy position, and the overall shape is the summarized contribution of all Mn valence states. Then

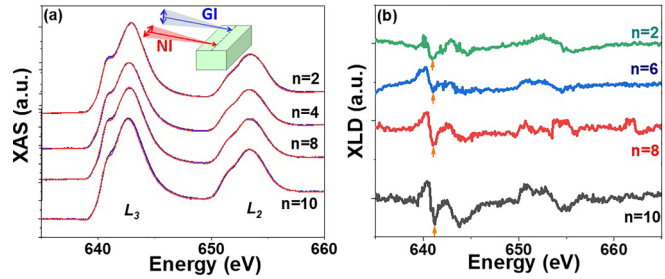

FIG. 8. (a) X-ray absorption spectrum (XAS) and (b) x-ray linear dichroism (XLD) measured at room temperature around the Mn $L_{3,2}$ edge for different n. The inset shows the configuration of the normal incident (NI) and grazing incident (GI) measurements.

the relative concentration of the Mn^{3+} ion should be high at the LSMO atomic layer connecting with the LAO atomic layer, which might come from the atomic diffusion/defect across the LSMO/LAO interface due to the high temperature during the fabrication process. When La^{3+} in the LAO layer diffuses into the LSMO layer by replacing Sr^{2+}, the chemical valence of Mn would decrease and the lattice constant would increase due to the large ionic radius of La^{3+}. This is consistent with the discussions above.

XLD in Fig. 8(b), which is the difference of XAS between GI and NI configurations $I_{\mathrm{XLD}} = I_{\mathrm{NI}} - I_{\mathrm{GI}}$, could measure the difference of occupancy in the two $3d$ e_g orbitals. The shape of XLD means a larger occupancy of the in-plane-oriented orbital $3d_{x^2-y^2}$ in $n = 2$, and the increasing dip at ~ 641 eV with increasing n indicates the gradual increasing occupancy of $3d_{3z^2-r^2}$ orbitals [30,31]. According to the crystal structure of the LSMO/LAO superlattice in Fig. 4, the out-of-plane lattice constant of the LSMO layer is smaller than the in-plane lattice constant, which would shift up the energy of the $3d_{3z^2-r^2}$ orbital with low occupancy, consistent with XLD measurement. With the suppressed probability of electron hopping along the out-of-plane direction with reduced intensity of magnetic exchange coupling, each atomic layer could behave independently and show multiple phase transitions, as observed. With the increase of n to 10, the innermost 4 LSMO atomic layers [Fig. 7(c)] with relatively higher c/a ratios and enhanced occupancy of $3d_{3z^2-r^2}$ orbitals, which would enlarge the electron hopping along out-of-plane direction, the interlayer interaction becomes strong, and these four atomic layers show only one phase transition (J_{10}), as observed above. For the phenomenon that the multiple phase transitions are missing during MT measurement with external magnetic field, it should be due to the relatively low anisotropy in the film plane [23]. Hence, the superlattice configuration with lattice mismatch could be exploited to explore the quasi-2D behavior of traditional 3D materials.

As is well known, the FM and AFM interactions coexist in manganite; the magnetic materials present a characteristic time dependence of the magnetization when the external magnetic field changes. During the magnetic relaxation process, multiplicity of available metastable states provides insights into the magnetic structure. The above discussion indicates that both the tetragonal ratio-dominated crystal structure and atomic/defect diffusion affect the materials properties. To

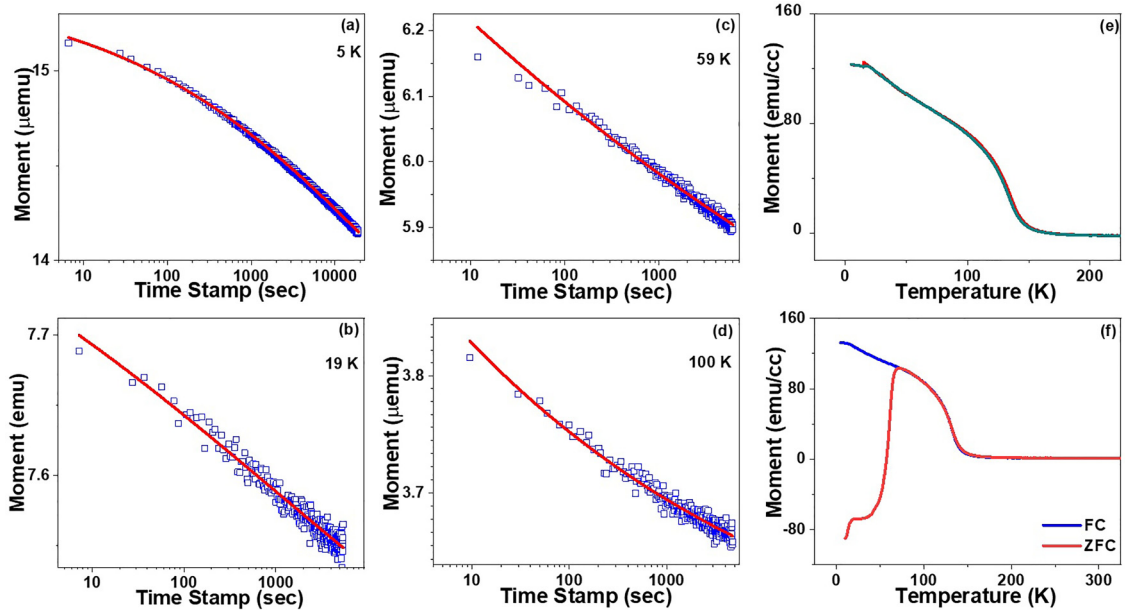

FIG. 9. (a)–(d) Time-dependent remnant magnetization (TRM) of $n = 4$ measured at different temperatures. The red line are fitting results according to the power law or logarithm law. (e) Magnetic memory effect and (f) zero-field cooling (ZFC) and field cooling (FC) magnetization-temperature (MT) curves for superlattice with $n = 4$.

study the effect of these factors on quasi-2D magnetic properties, the sample $n = 4$ with only two phase transitions was studied at different temperatures. Figures 9(a)–9(d) show the time-dependent remnant magnetization (TRM) [32] at different temperatures. As can been seen, the TRM curve at the magnetic phase with a higher phase transition (>15 K) follows the power-law decay [33] $m(t) = m_0 + m_1 t^{-\eta}$ with η decreasing with decreasing temperature, which depends on the density of the FM cluster in the LSMO atomic layer and hence on the strength of the intercluster interaction. With further decreasing temperature to 5 K, where the magnetic phase with lower phase transition temperature contribute to the overall properties, the TRM curve follows the logarithm decay [34] $m(t) = m_0 - m_1 \exp[-(t/t_0)^{1-n}]$, which normally occurs in systems without intercluster interactions. The different decay laws at these two magnetic phases suggest that the absence of intercluster interaction contributes to the deterioration of magnetic properties at the interface.

The FC and zero-FC (ZFC) MT diverges at the maximum of the ZFC curve, which suggests uniform distribution of the magnetic cluster size [35]. In addition, the ZFC curves show two sharp jumps of magnetism, corresponding to two magnetic phases. Then the memory effect in magnetic properties [36] was measured in Fig. 9(e) to provide more information on the cluster behavior. The red MT curve of superlattices was measured during cooling from 300 to 5 K under a magnetic field of 100 Oe. During the measurement, it stops for 2.5 h at 30 and 14 K with magnetic field off, respectively. Due to the relaxation of magnetization, a steplike downturn in the MT curve appears at 14 K. After cooling, a MT curve during the warming process was measured without stopping at any temperature. The measurements clearly show the memory effect at 14 K with magnetic properties dominated by the outermost 2D-LSMO atomic layer connecting with LAO directly: The warming MT curve shows anomalous upturns at 14 K with magnetization recovering back to the value observed during the cooling process. This observed memory effect reveals that the metastable states are established and frozen during the cooling process. Melting of these states during the warming process induces anomalous features of magnetization at the same stopping temperatures. At 30 K, with magnetic properties dominated by the inner 2D-LSMO atomic layer, the memory effect is quite weak. The results suggest the existence of spin frustration [37] is exaggerated at the outermost 2D-LSMO atomic layer without intercluster (dipole-dipole) interaction, which should be responsible for the significantly weakened interaction at this LSMO atomic layer (magnetic dead layer). Combining the above discussion, the magnetic dead layer mostly is constrained at the outermost 2D-LSMO atomic layer connecting with LAO directly, illustrated as green bars in Fig. 7(c), which is different from a single LSMO layer on a STO substrate ~7 u.c. [38]. Between the superlattice and a single layer, the interface components and the coupling to strain are different, resulting in different magnetic dead layers. Hence, the superlattice configuration could be exploited to control the quasi-2D behavior of the LSMO layer and improve the magnetic properties.

IV. CONCLUSIONS

In this paper, the LSMO/LAO superlattice with n unit cells for each layer in one period was investigated. The number of magnetic phase transitions has a close relationship with the number of unit cells (n): only one phase transition for $n = 2$ and four phase transitions for $n = 8$. Further study shows that the local structure with the corresponding electronic structure of each 2D-$La_{0.7}Sr_{0.3}MnO_3$ atomic layer was responsible for the multiple phase transitions. In this paper, we demonstrate

that the quasi-2D behavior of the manganite film could be induced in the superlattice, which could be applicable in other system.

ACKNOWLEDGMENTS

The research was supported by the National Natural Science Foundation of China under Grant No. 11904415 and No. 11972382, the Natural Science Foundation of Guangdong Province, China under Grant No. 2023A1515010882, the Large Scientific Facility Open Subject of Songshan Lake, Dongguan, Guangdong under Grant No. KFKT2022B06, Fundamental Research Funds for the Central Universities under Grant No. 19lgpy265, and Startup Grant (No. 74130-18841221); H.Z. is supported by National Natural Science Foundation of China under Grant No. 12274185; the Singapore Ministry of Education Academic Research Fund Tier 2 under the Projects No. MOE2015-T2-1-016 and MOE2018-T2-1-019, MoE T1 R-284-000-196-114, and the Singapore National Research Foundation under CRP Award No. NRF-CRP10-2012-02. P.Y. is supported from SSLS via NUS Core Support C-380-003-003-001.

The authors declare no conflict of interest.

[1] B. Chen, N. Gauquelin, D. Jannis, D. M. Cunha, U. Halisdemir, C. Piamonteze, J. H. Lee, J. Belhadi, F. Eltes, S. Abel *et al.*, Strain-engineered metal-to-insulator transition and orbital polarization in nickelate superlattices integrated on silicon, Adv. Mater. **32**, 2004995 (2020).

[2] M. Ye, S. Hu, Y. Zhu, Y. Zhang, S. Ke, L. Xie, Y. Zhang, S. Hu, D. Zhang, Z. Luo *et al.*, Electric polarization switching on an atomically thin metallic oxide, Nano Lett. **21**, 144 (2021).

[3] D. Li, K. Lee, B. Y. Wang, M. Osada, S. Crossley, H. R. Lee, Y. Cui, Y. Hikita, and H. Y. Hwang, Superconductivity in an infinite-layer nickelate, Nature **572**, 624 (2019).

[4] C. Liu, Y. Liu, B. Zhang, C.-J. Sun, D. Lan, P. Chen, X. Wu, P. Yang, X. Yu, T. Charlton *et al.*, Ferroelectric self-polarization controlled magnetic stratification and magnetic coupling in ultrathin $La_{0.67}Sr_{0.33}MnO_3$ films, ACS Appl. Mater. Interfaces **13**, 30137 (2021).

[5] Y. Zhang, K. Shinokita, K. Watanabe, T. Taniguchi, M. Goto, D. Kan, Y. Shimakawa, Y. Moritomo, T. Nishihara, Y. Miyauchi *et al.*, Controllable magnetic proximity effect and charge transfer in 2D semiconductor and double-layered perovskite manganese oxide van der Waals heterostructure, Adv Mater. **32**, 2003501 (2020).

[6] D. Yi, J. Liu, S. L. Hsu, L. Zhang, Y. Choi, J. W. Kim, Z. Chen, J. D. Clarkson, C. R. Serrao, E. Arenholz *et al.*, Atomic-scale control of magnetic anisotropy via novel spin-orbit coupling effect in $La_{2/3}Sr_{1/3}MnO_3/SrIrO_3$ superlattices, Proc. Natl. Acad. Sci. USA **113**, 6397 (2016).

[7] W. Lin, L. Li, F. Dogan, C. Li, H. Rotella, X. Yu, B. Zhang, Y. Li, W. S. Lew, S. Wang *et al.*, Interface-based tuning of Rashba spin-orbit interaction in asymmetric oxide heterostructures with 3*d* electrons, Nat. Commun. **10**, 3052 (2019).

[8] N. Nakagawa, H. Y. Hwang, and D. A. Muller, Why some interfaces cannot be sharp, Nat. Mater. **5**, 204 (2006).

[9] B. Chen, H. Xu, C. Ma, S. Mattauch, D. Lan, F. Jin, Z. Guo, S. Wan, P. Chen, G. Gao *et al.*, All-oxide–based synthetic antiferromagnets exhibiting layer-resolved magnetization reversal, Science **357**, 191 (2017).

[10] E. Dagotto, T. Hotta, and A. Moreo, Colossal magnetoresistant materials: The key role of phase separation, Phys. Rep. **344**, 1 (2001).

[11] X. Zhai, L. Cheng, Y. Liu, C. M. Schleputz, S. Dong, H. Li, X. Zhang, S. Chu, L. Zheng, J. Zhang *et al.*, Correlating interfacial octahedral rotations with magnetism in $(LaMnO_{3+\delta})_N/(SrTiO_3)_N$ superlattices, Nat. Commun. **5**, 4283 (2014).

[12] E. J. Moon, R. Colby, Q. Wang, E. Karapetrova, C. M. Schleputz, M. R. Fitzsimmons, and S. J. May, Spatial control of functional properties via octahedral modulations in complex oxide superlattices, Nat. Commun. **5**, 5710 (2014).

[13] B. Zhang, C.-J. Sun, P. Yang, W. Lu, B. L. Fisher, T. Venkatesan, S. M. Heald, J.-S. Chen, and G. M. Chow, Strain modulated anisotropic electronic charge transfer in perovskite $Pr_{0.67}Sr_{0.33}MnO_3$ thin films, Phys. Rev. B **89**, 195140 (2014).

[14] Y. Tokura, Critical features of colossal magnetoresistive manganites, Rep. Prog. Phys. **69**, 797 (2006).

[15] B. Zhang, L. Wu, W. G. Yin, C. J. Sun, P. Yang, T. Venkatesan, J. Chen, Y. Zhu, and G. M. Chow, Interfacial coupling-induced ferromagnetic insulator phase in manganite film, Nano Lett. **16**, 4174 (2016).

[16] M. I. Marqués, C. Aragó, and J. A. Gonzalo, Quantum paraelectric behavior of $SrTiO_3$: Relevance of the structural phase transition temperature, Phys. Rev. B **72**, 092103 (2005).

[17] D. V. Christensen, Y. Frenkel, Y. Z. Chen, Y. W. Xie, Z. Y. Chen, Y. Hikita, A. Smith, L. Klein, H. Y. Hwang, N. Pryds *et al.*, Strain-tunable magnetism at oxide domain walls, Nat. Phys. **15**, 269 (2018).

[18] A. J. Millis, P. B. Littlewood, and B. I. Shraiman, Double Exchange Alone Does Not Explain the Resistivity of $La_{1-x}Sr_xMnO_3$, Phys. Rev. Lett. **74**, 5144 (1995).

[19] M. R. Khan, C. S. L. Chun, G. P. Felcher, M. Grimsditch, A. Kueny, C. M. Falco, and I. K. Schuller, Structural, elastic, and transport anomalies in molybdenum/nickel superlattices, Phys. Rev. B **27**, 7186 (1983).

[20] A. Vailionis, H. Boschker, Z. Liao, J. R. A. Smit, G. Rijnders, M. Huijben, and G. Koster, Symmetry and lattice mismatch induced strain accommodation near and away from correlated perovskite interfaces, Appl. Phys. Lett. **105**, 131906 (2014).

[21] R. Mishra, Y. M. Kim, J. Salafranca, S. K. Kim, S. H. Chang, A. Bhattacharya, D. D. Fong, S. J. Pennycock, S. T. Pantelides, and A. Y. Borisevich, Oxygen-vacancy-induced polar behavior in $(LaFeO_3)_2/(SrFeO_3)$ superlattices, Nano Lett. **14**, 2694 (2014).

[22] A. J. Millis, T. Darling, and A. Migliori, Quantifying strain dependence in "colossal" magnetoresistance manganites, J. Appl. Phys. **83**, 1588 (1998).

[23] H. S. Wang, E. Wertz, Y. F. Hu, Q. Li, and D. G. Schlom, Role of strain in magnetotransport properties of $Pr_{0.67}Sr_{0.33}MnO_3$ thin films, J. Appl. Phys. **87**, 7409 (2000).

[24] Z. Wang, H. Guo, S. Shao, M. Saghayezhian, J. Li, R. Fittipaldi, A. Vecchione, P. Siwakoti, Y. Zhu, J. Zhang *et al.*, Designing an-

tiphase boundaries by atomic control of heterointerfaces, Proc. Natl. Acad. Sci. USA **115**, 9485 (2018).

[25] Z. Wang, J. Tao, L. Yu, H. Guo, L. Chen, M.-G. Han, L. Wu, H. Xin, K. Kisslinger, E. W. Plummer *et al.*, Anomalously deep polarization in $SrTiO_3$ (001) interfaced with an epitaxial ultrathin manganite film, Phys. Rev. B **94**, 155307 (2016).

[26] M. N. Grisolia, J. Varignon, G. Sanchez-Santolino, A. Arora, S. Valencia, M. Varela, R. Abrudan, E. Weschke, E. Schierle, J. E. Rault *et al.*, Hybridization-controlled charge transfer and induced magnetism at correlated oxide interfaces, Nat. Phys. **12**, 484 (2016).

[27] T. Kanki, H. Tanaka, and T. Kawai, Anomalous strain effect in $La_{0.8}Ba_{0.2}MnO_3$ epitaxial thin film: Role of the orbital degree of freedom in stabilizing ferromagnetism, Phys. Rev. B **64**, 224418 (2001).

[28] R. U. Chandrasena, W. Yang, Q. Lei, M. U. Delgado-Jaime, K. D. Wijesekara, M. Golalikhani, B. A. Davidson, E. Arenholz, K. Kobayashi, M. Kobata *et al.*, Strain-engineered oxygen vacancies in $CaMnO_3$ thin films, Nano Lett. **17**, 794 (2017).

[29] K. Huang, L. Wu, M. Wang, N. Swain, M. Motapothula, Y. Luo, K. Han, M. Chen, C. Ye, A. J. Yang *et al.*, Tailoring magnetic order via atomically stacking $3d/5d$ electrons to achieve high-performance spintronic devices, Appl. Phys. Rev. **7**, 011401 (2020).

[30] C. Liu, B. Zhang, X. Yu, X. Wu, P. Chen, P. Yang, X. Yu, J. Ding, J. Chen, and G. M. Chow, Magnetoelectric coupling induced orbital reconstruction and ferromagnetic insulating state in $PbZr_{0.52}Ti_{0.48}O_3/La_{0.67}Sr_{0.33}MnO_3$ heterostructures, ACS Appl. Mater. Interfaces **12**, 35588 (2020).

[31] D. Pesquera, G. Herranz, A. Barla, E. Pellegrin, F. Bondino, E. Magnano, F. Sánchez, and J. Fontcuberta, Surface symmetry-breaking and strain effects on orbital occupancy in transition metal perovskite epitaxial films, Nat. Commun. **3**, 1189 (2012).

[32] M. Sasaki, P. E. Jönsson, H. Takayama, and H. Mamiya, Aging and memory effects in superparamagnets and superspin glasses, Phys. Rev. B **71**, 104405 (2005).

[33] E. Bose and S. Pal, Investigation of low-temperature magnetic relaxation and intercluster interaction in electron-doped $Ca_{0.85}La_{0.15}MnO_3$ manganite, J. Supercond. Novel Magn. **30**, 1899 (2017).

[34] V. A. Desnenko, V. A. Sirenko, I. O. Troyanchuk, A. V. Fedorchenko, and A. V. Yeremenko, Low-temperature relaxation of magnetization in manganite $Pr_{0.4}Bi_{0.3}Ca_{0.3}MnO_3$, Low Temp. Phys. **44**, 962 (2018).

[35] I. G. Deac, S. V. Diaz, B. G. Kim, S. W. Cheong, and P. Schiffer, Magnetic relaxation in $La_{0.250}Pr_{0.375}Ca_{0.375}MnO_3$ with varying phase separation, Phys. Rev. B **65**, 174426 (2002).

[36] M. Bandyopadhyay and S. Dattagupta, Memory in nanomagnetic systems: Superparamagnetism versus spin-glass behavior, Phys. Rev. B **74**, 214410 (2006).

[37] J. Ding, F. Cossu, O. I. Lebedev, Y. Zhang, Z. Zhang, U. Schwingenschlögl, and T. Wu, Manganite/cuprate superlattice as artificial reentrant spin glass, Adv. Mater. Interfaces. **3**, 1500676 (2016).

[38] M. Huijben, L. W. Martin, Y. H. Chu, M. B. Holcomb, P. Yu, G. Rijnders, D. H. A. Blank, and R. Ramesh, Critical thickness and orbital ordering in ultrathin $La_{0.7}Sr_{0.3}MnO_3$ films, Phys. Rev. B **78**, 094413 (2008).